NUMERICAL ANALYSIS OF UNSTEADY THREE-DIMENSIONAL FLOW IN A PROPELLER FAN USING MULTI-SCALE LATTICE BOLTZMANN METHOD

Kazuya KUSANO[1], Kazutoyo YAMADA[2], Masato FURUKAWA[2]

[1] *Hitachi, Ltd., Hitachi Research Laboratory, 832-2, Horiguchi, Hitachinaka, Ibaraki, Japan*

[2] *Department of Mechanical Engineering, Kyushu University, 744 Motooka, Nishi-ku, Fukuoka, Japan*

SUMMARY

The present paper provides validation results of the lattice Boltzmann method (LBM) for the simulation of a complicated flow field around a propeller fan. In the present numerical simulation, solid boundaries of the rotor and the shroud were calculated by a simple immersed boundary scheme. The computational grid around the propeller fan was generated by the Building-Cube Method (BCM). Furthermore, the multi-scale model was introduced into the LBM to allow the calculation with such grids. The LBM result agreed well with the experimental result and the result of detached eddy simulation (DES) which solved the Navier-Stokes equations. It confirmed that the present approach was effective for flow simulations of propeller fans using LBM.

INTRODUCTION

Reduction of turbulent flow noise is a crucial issue in fans. For better prediction of broadband noise with high frequency, which is generally generated in high Reynolds number flows, not only high grid resolution is required to capture very small eddies of the sound sources inside the turbulent boundary layer, but also the computation of acoustic field is often needed. In such case, the direct simulation of flow field and acoustic field is straightforward and effective. The lattice Boltzmann method (LBM) is suitable for such simulation thanks to its advantages. The algorithm of the LBM is simple and easy-to-parallelization, compared to that of the conventional CFD methods solving Navier-Stokes equations. In fact, the capability of the LBM in aeroacoustic computations for low Mach number flows has been reported [1, 2].

In turbomachinery field, the conventional Navier-Stokes simulation is more common. Recently, a few applications of LBM to low speed fans [3, 4] can be seen. The commercial code PowerFlow was used in those studies. PowerFlow adapted Very Large Eddy Simulation (VLES) as a turbulence model. In VLES, the turbulent boundary layer calculated by a wall-model using a coarse mesh.

The goal of this study is to establish the prediction method of turbulent flow noise radiated from low speed fans using the LBM. For the prediction of broadband noise with high frequency, turbulent wall-model was not used, and eddies in the turbulent boundary layer was simulated as directly as possible using a higher resolution mesh than the conventional studies [3, 4]. The present paper provides the validation result of the LBM for a complicated flow field around a propeller fan. The present simulation was performed by an in-house code.

TEST FAN

The test fan is a half-ducted propeller fan, which is used as a cooling fan installed in an outdoor unit of room air conditioner. Figure 1 shows the configuration of the test fan. As shown in Figure 1, the fan consists of a rotor and a shroud covering only the rear region of the rotor tip. Table 1 shows the design specifications of the test propeller fan. The Reynolds number based on the tip radius and the rotor tip speed is 2.6×10^5. The Mach number of the rotor tip is 0.05.

NUMERICAL ANALYSIS METHOD

Lattice Boltzmann Method

The basic equation is the lattice BGK equation with the force term [5], which is written as

$$f_i(t+\Delta t, \mathbf{x}+\Delta t\mathbf{c}_i) = f_i(t,\mathbf{x}) - \frac{1}{\tau}\left[f_i(t,\mathbf{x}) - f_i^{\mathrm{eq}}(t,\mathbf{x})\right] + \Delta t T_i , \quad (1)$$

where f is the particle distribution function, $\boldsymbol{c}$ is the particle velocity, f^{eq} is the locale equilibrium velocity distribution function, τ is the single relaxation time, and the subscript i represents the direction of particles' motion. Fluid density and momentum are defined as follows:

$$\rho = \sum_i f_i \quad (2)$$

$$\rho\mathbf{u} = \sum_i f_i\mathbf{c}_i + \frac{\Delta t}{2}\mathbf{F} , \quad (3)$$

where **F** is the body force. The single relaxation time τ has a relation with the kinematic viscosity,

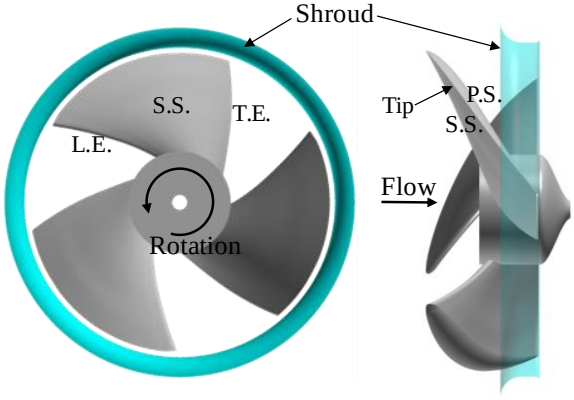

Figure 1: Test propeller fan

Table 1: Design specifications of test propeller fan

Number of blade Z_b	3
Tip radius r_{tip}	235mm
Rotor rotation frequency N	683rmp
Hub-tip ratio ν	0.3404
Tip clearance	7.76mm
Chord length at tip	353mm
Solidity at tip	0.72
Flow coefficient ϕ	0.291
Static pressure rise coefficient ψ	0.130

which can be written as the following equation.

$$\nu = \frac{1}{3}\left(\tau - \frac{1}{2}\right)\Delta t c^2 \tag{4}$$

As a discrete velocity model, the D3Q15 model was used in the present simulation. The local equilibrium velocity distribution function for the D3Q15 model is given as follows:

$$f_i^{\mathrm{eq}} = w_i \rho \left[1 + 3\mathbf{c}_i \cdot \mathbf{u} + \frac{9}{2}(\mathbf{c}_i \cdot \mathbf{u})^2 - \frac{3}{2}\mathbf{u} \cdot \mathbf{u}\right] \tag{5}$$

where w_i is the weighting factor, which is defined as $w_0 = 2/9$, $w_{1\sim6} = 1/9$, $w_{7\sim14} = 1/72$. The forcing term T_i in the equation (1) is given by the following equation.

$$T_i = \left(1 - \frac{1}{2\tau}\right) w_i \left[\frac{\mathbf{c}_i - \mathbf{u}}{c_s^{\,2}} + \frac{\mathbf{c}_i \cdot \mathbf{u}}{c_s^{\,4}}\mathbf{c}_i\right] \cdot \mathbf{F} \tag{6}$$

In the rotating frame, **F** corresponds to the centrifugal force and the Coriolis force.

Multi-scale Model

In the standard LBM, simulations are conducted using the regular lattice with uniform spacing. To make the LBM suitable for practical use, a function of utilizing locally refined grids is essential. In the present study, the multi-scale model [6] has been introduced to the LBM. The multi-scale LBM can use grids which are fine locally around the object, while still retaining its advantages such as simple algorithm and straightforward to be parallelized.

In order to ensure continuity of the variables such as density and momentum and their derivatives at the interface between the coarse and fine grids, the scales of the distribution function are transformed by the following equations.

$$\hat{f}_i^{\,\mathrm{f}} = f_i^{\mathrm{eq,c}} - \frac{1}{\Omega}(\hat{f}_i^{\,\mathrm{c}} - f_i^{\mathrm{eq,c}}) \tag{7}$$

$$\hat{f}_i^{\,\mathrm{c}} = f_i^{\mathrm{eq,f}} - \Omega(\hat{f}_i^{\,\mathrm{f}} - f_i^{\mathrm{eq,f}}) \tag{8}$$

The superscripts of "f" and "c" represent the distribution functions in the coarse and fine grids, respectively. $\hat{f}$ is the distribution function after the collision operation. Also, Ω is the parameter defined as follow:

$$\Omega = n\frac{\tau^{\mathrm{c}} - 1}{\tau^{\mathrm{f}} - 1}, \tag{9}$$

where n is the ratio of coarse to fine grid spacing. In the present study, n was set to two.

Figure 2 is a description of the computational procedure at the interface between the coarse and fine grids. As shown in Figure 2, grid points are overlapped in the interface. First, the collision operation is conducted in each grid. After that, spatial interpolations are implemented for the distribution functions in the coarse grid. Because the time step size in the coarse grid is larger than that in the fine grid, temporal interpolations are also implemented at the interface of the coarse grid. Next, the scale transformations in the coarse grid and the fine grid are implemented using the equations (7) and (8), respectively. Finally, the streaming operation is implemented. This is how the exchange of the distribution functions over the interface is completed.

Boundary Conditions

The Interpolated Bounce-Back scheme [7] was used as a solid boundary condition. This scheme can achieve high accuracy than the standard Bounce-Back scheme with a little increase in computation procedure. Figure 3 shows a description of the Interpolated Bounce-Back scheme. In Figure 3, $\boldsymbol{x}_s$ represents the position of a node which is located inside a body and the nearest to the body surface. The solid boundary condition is given to this node. $\boldsymbol{x}_1$ is the position of a first node from the body surface in a fluid region and $\boldsymbol{x}_2$ is a second node. q_i represents the distance between the solid surface and $\boldsymbol{x}_1$. It is assumed that the particle on the red point reaches to $\boldsymbol{x}_1$ at the next time step. The distribution function on the red point at the present time step can be calculated by the interpolation, and then it can be given to $\boldsymbol{x}_s$ as a boundary condition. The distribution functions are interpolated as follows:

$$\hat{f}_{\bar{i}}(t,\mathbf{x}_s)=\frac{2q_i}{\Delta x}\,\hat{f}_i(t,\mathbf{x}_1)+\frac{(\Delta x-2q_i)}{\Delta x}\,\hat{f}_i(t,\mathbf{x}_2),\quad (q_i<\Delta x/2) \tag{10}$$

$$\hat{f}_{\bar{i}}(t,\mathbf{x}_s)=\frac{\Delta x}{2q_i}\,\hat{f}_i(t,\mathbf{x}_1)+\frac{(2q_i-\Delta x)}{2q_i}\,\hat{f}_{\bar{i}}(t,\mathbf{x}_1),\quad (q_i\geq\Delta x/2)\,, \tag{11}$$

where $\bar{\imath}$ represents the opposite direction to i.

At the nodes of the inlet boundary, the local equilibrium distribution function calculated by inlet

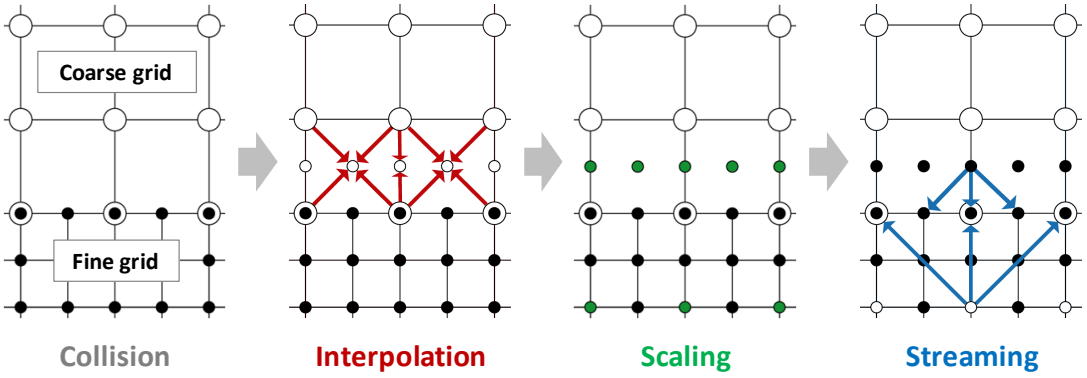

Figure 2: Computational procedure in interface between two blocks of different lattice spacing

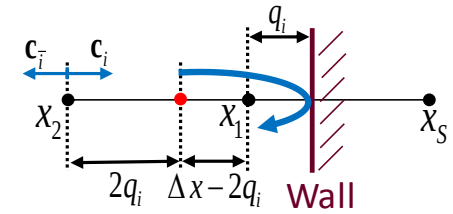

(a) $q_i < \Delta x/2$

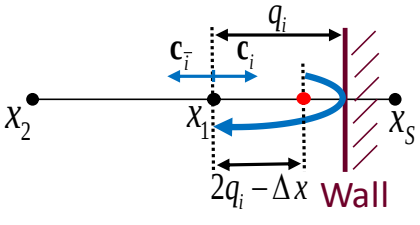

(b) $q_i \geq \Delta x/2$

Figure 3: Illustration of the interpolated Bounce-Back scheme

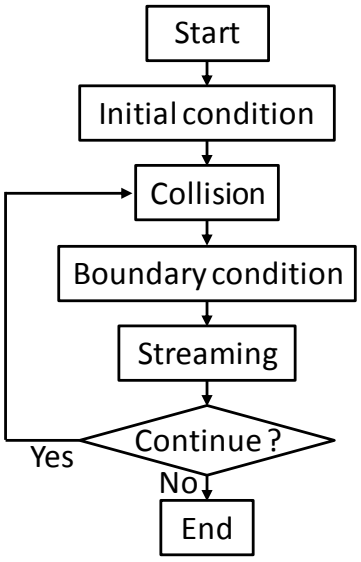

Figure 4: Computational procedure of LBM

density and velocity was specified. The inlet axial velocity was calculated from the flow rate, and the radial and circumferential velocity were set to 0[m/s]. Also, as the outlet boundary, the local equilibrium distribution function was specified. The outlet density and velocity were extrapolated from inner nodes. The extrapolated density and velocity were used for the calculation of the local equilibrium distribution function.

Filtering Operation

Simulations of high Reynolds number flow using the LBM suffer from numerical instabilities in the region of coarse grids, because the relaxation time becomes small there. In the present study, the filtering operation was used for the distribution function to eliminate numerical oscillations with high frequencies. The filtering scheme is expressed by the following equation [8].

$$a_f \tilde{f}_i(t,\mathbf{x}-\mathbf{c}_i\Delta t)+\tilde{f}_i(t,\mathbf{x})+a_f \tilde{f}_i(t,\mathbf{x}+\mathbf{c}_i\Delta t)=\sum_{n=0}^{N}\frac{a_n}{2}(f_i(t,\mathbf{x}-n\Delta t\mathbf{c}_i)+f_i(t,\mathbf{x}+n\Delta t\mathbf{c}_i)) \quad (12)$$

In the present study, the fourth-order scheme (N = 2) was used. a_f is a free parameter specified in range of $-0.5 < a_f \leq 0.5$. In the present simulation, a_f was set to 0.45.

Computational Grid

The computational grid was generated by the Building-Cube Method (BCM) proposed by Nakahashi et al. [9]. The BCM divides a computational domain into multiple cubes of various sizes. By allocating small cubes to the vicinity of a body, the BCM generates locally refined grids. The grids generated by the BCM are available for LBM computations, because each cube has a regular lattice with uniform spacing. Also, all cubes have the same number of grid points. Therefore, it is easy to distribute computational tasks across multiple processors. In the present simulation, the computation was parallelized with the region-dividing technique using MPI.

Figure 5 shows the computational domain and the distribution of cubes on the meridional plane. As shown in Figure 5, the propeller fan is placed between the inlet and outlet chamber. The red region was calculated in the reference frame which rotates with the rotor. On the other hand, the blue region was calculated in the stationary frame. Figure 6 displays the computational grid around the propeller fan. In the figure, the grid is described by every eight lines. It is observed that the grid has a high resolution near the rotor and the shroud. The minimum value of grid spacing normalized by the tip radius is 9.8×10^{-4}, which equals to 12 in the wall unit. The total number of cubes is 46,580. Each cube has 33^3 grid points. It follows that the number of grid points is 1.67 billion in total.

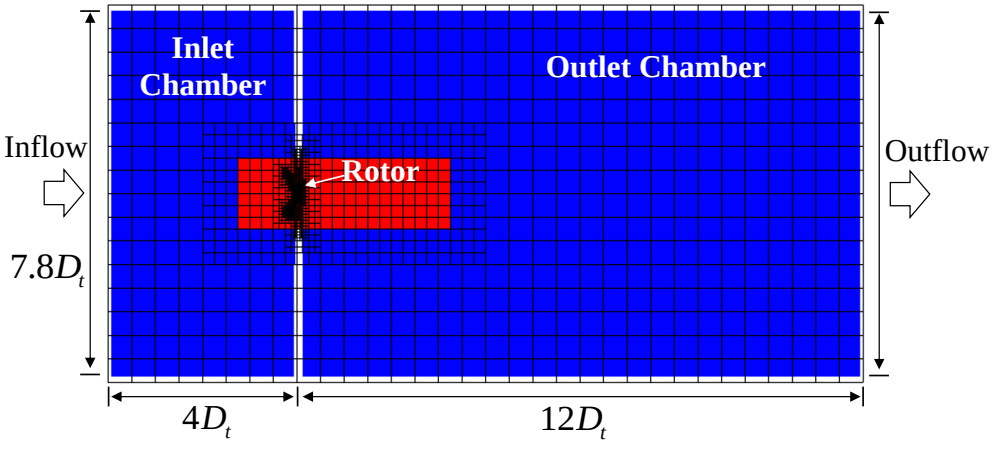

Figure 5: The computational domain and distribution of cubes on meridional plane

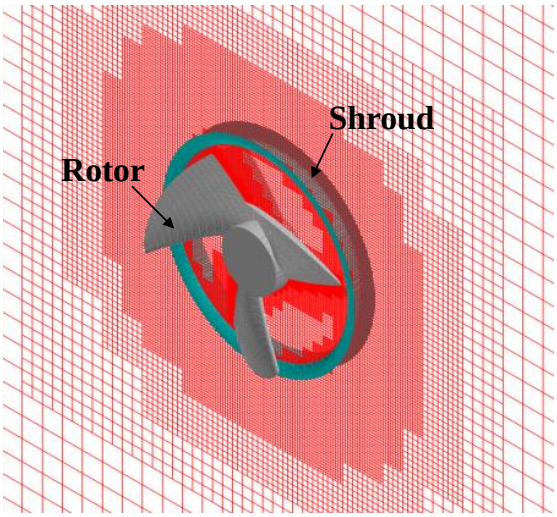

Figure 6: The computational grid around the propeller fan

RESULTS AND DISCUSSION

In this section, the experimental results and the DES results [10, 11] were used for the validation of the LBM results. Figure 7 shows time-averaged velocity distributions downstream of the rotor obtained by the LDV measurement and the LBM calculation, respectively. In Figure 7, the white circle indicates the position of the tip vortex center. The position of the tip vortex center of LBM is in good agreement with that of LDV. Also, the LBM results have captured the distinctive features in the velocity distributions induced by the tip vortex. In axial velocity distributions of Figure 7 (a) and (d), low velocity region, which is surrounded by black dashed lines, corresponds to the corner separation between the blade suction surface and the hub. All velocity components near the corner separation of the LBM results have good agreements with those of the LDV results.

The computational result by the LBM was compared with the result by the detached eddy simulation which solved Navier-Stokes equations using a body-fitted grid. Figure 8 shows three-dimensional vortex structures in time-averaged flow fields. Vortex structures were identified by the semi-analytic method developed by Sawada [12], which is based on the critical-point theory. In the figure, identified vortex structures are colored with the normalized helicity. In Figure 8 (a), the tip vortex is formed near the leading edge on the suction side of the blade, and it convects nearly along the suction surface in the un-ducted region. When the tip vortex reaches the shroud, then it turns in the tangential direction under the influence of the shroud surface. The LBM result of Figure 8 (a) is consistent with the DES result of Figure 8 (a) in terms of the trajectory of the tip vortex.

Figure 9 shows the distributions of turbulence level downstream of the rotor. The turbulence level *T.L.* is defined as follows:

$$T.L. = \sqrt{\frac{c_z'^2 + c_r'^2 + c_\theta'^2}{3U_t^2}} \tag{13}$$

where c_z' , c_r' and c_θ' denote the velocity fluctuation components in the axial, radial and circumferential directions, respectively. U_t is the speed of the rotor tip. In the LDV result, the highest turbulence is observed around the tip vortex. The other high turbulence regions are located in the rotor blade wake and the corner separation, and between the blade wake and the tip vortex. These four high turbulence regions can be identified in the LBM result. However, the LBM result shows higher turbulence level than the LDV result. It is assumed that the present grid resolution is still insufficient for directly simulating small-scale eddies of the turbulent flow.

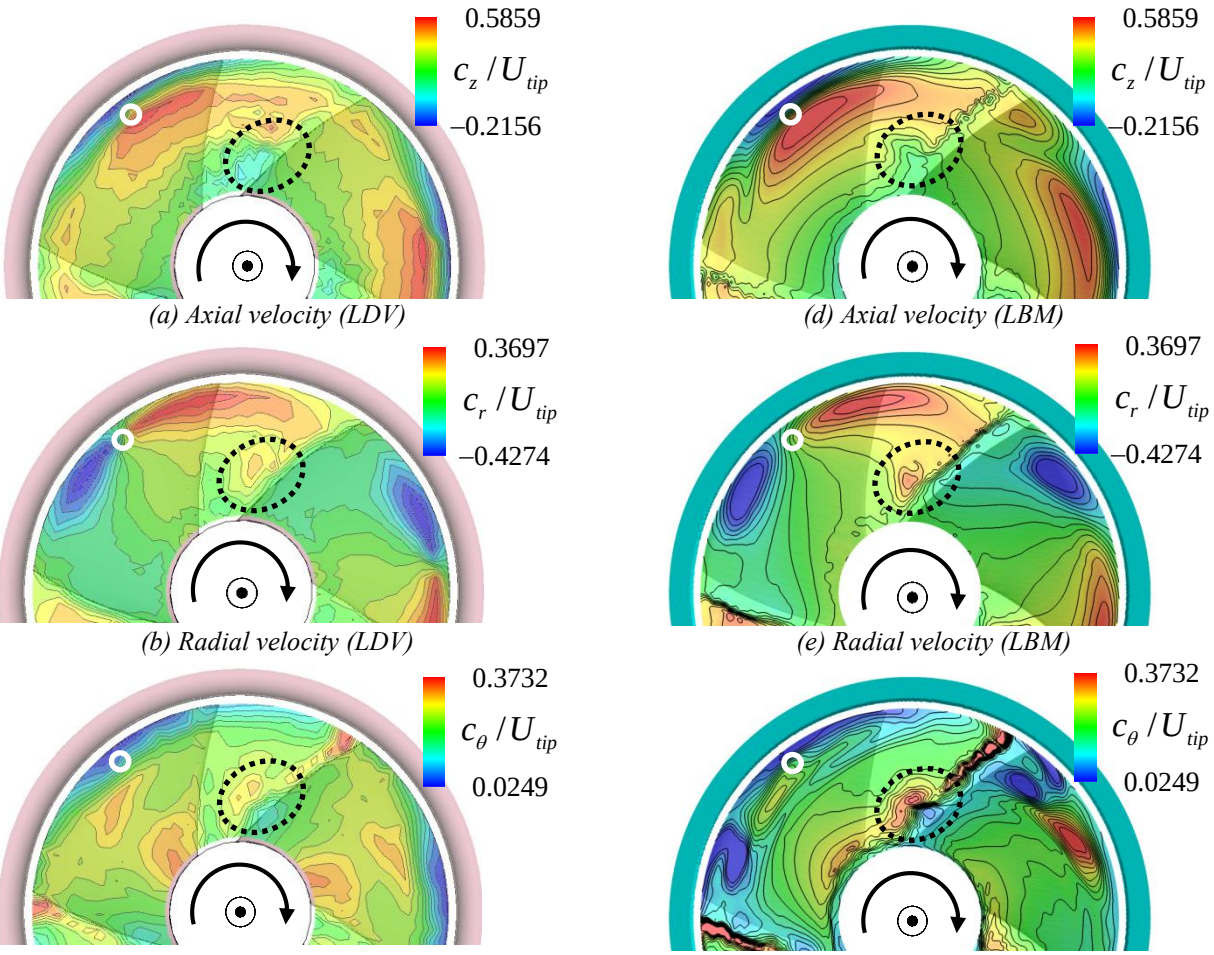

(a) Axial velocity (LDV) *(d) Axial velocity (LBM)*

(b) Radial velocity (LDV) *(e) Radial velocity (LBM)*

(c) Circumferential velocity (LDV) *(f) Circumferential velocity (LBM)*

Figure 7: Time-averaged velocity distributions downstream of the rotor

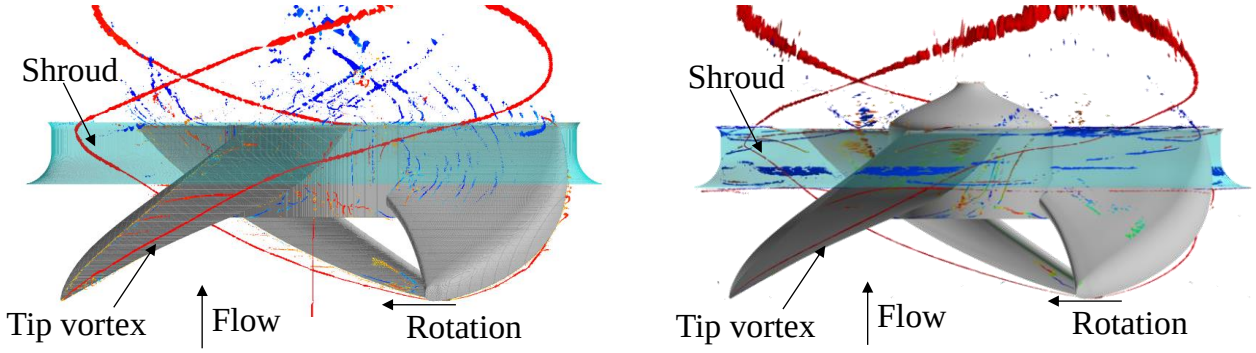

(a) LBM *(b) DES*

Figure 8: Time-averaged vortex structures

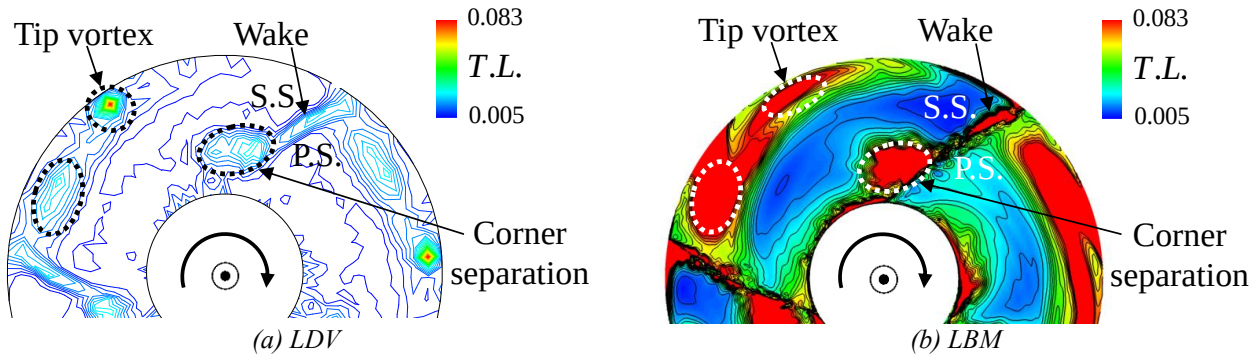

(a) LDV *(b) LBM*

Figure 9: Turbulence level distributions downstream of the rotor

Figure 10 compares pressure fluctuation on the blade suction surface between the experimental result and the LBM result. It is important to capture dipole sources on the wall for prediction of aerodynamic sounds in low speed fans. In Figure 10, the highest pressure fluctuation is observed near the leading edge of the tip region in the both results. Three-dimensional vortex structures in an instantaneous flow field are shown in Figure 11. Several small eddies are identified on the suction surface near the leading edge of the tip region. It is suspected that the laminar flow which has been separated on the leading edge becomes turbulent and reattaches to the blade surface around the above-mentioned region. Also, it is observed that other small vortices shed from the blade tip run into the tip vortex in the un-ducted region. The structure of the tip vortex is not identified clearly in the instantaneous flow filed of Figure 11, compared to that in the time-averaged flow field of Figure 8 (a). This is caused by unsteady fluctuation of vorticity in the tip vortex. In Figure 10 (a) and (b), the high pressure fluctuation seen near the mid-chord of the tip region can be attributed to this unsteady nature of the tip vortex. The high pressure fluctuation near the rear part of the tip region in the LBM result of Figure 10 (b) can be caused by the unsteady rolling-up of the tip leakage vortex between the blade tip and the shroud. In the experimental result of Figure 10 (a), it was not captured due to the lack of measurement points. In addition, the high pressure fluctuation seen near the blade

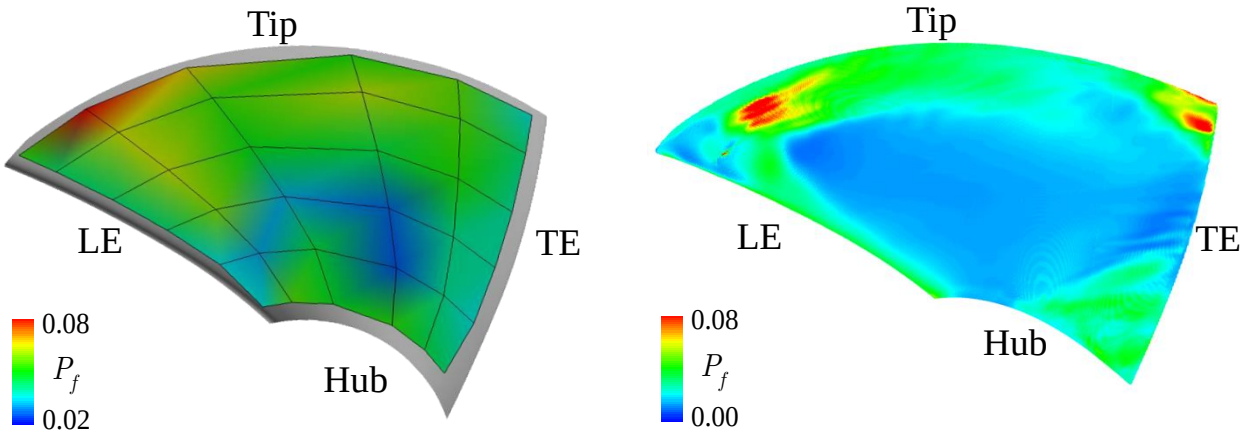

(a) EXP *(b) LBM*

Figure 10: Distributions of Pressure fluctuation on the blade suction surface

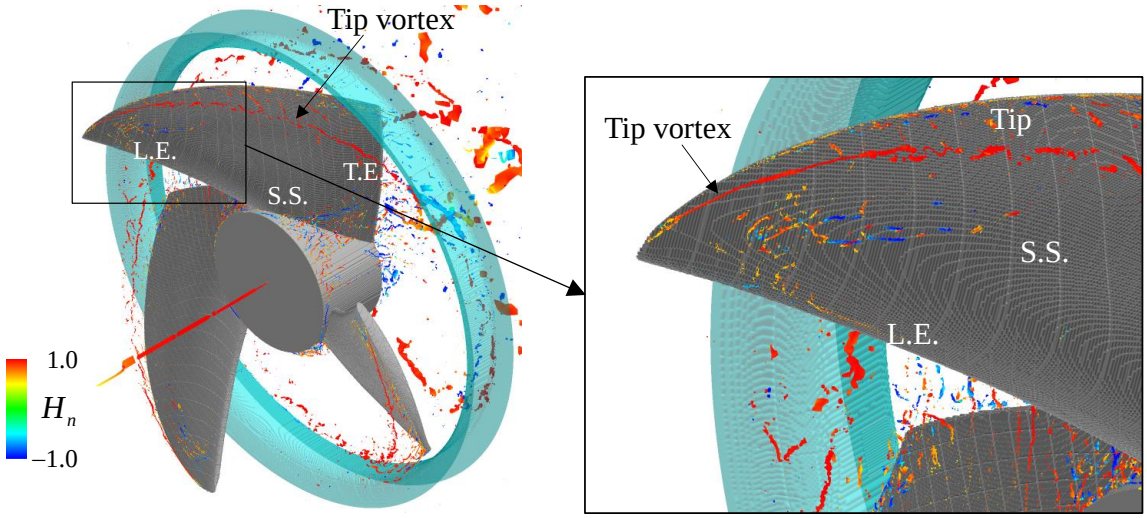

Figure 11: Instantaneous vortex structures

root in Figure 10 (a) and (b) is interpreted as due to the unsteady interaction of the corner separation vortices, which are seen in the corner between the blade suction surface and the hub of Figure 11. As shown above, the LBM result has good agreements with the experimental result in the blade pressure fluctuation.

CONCLUSIONS

The numerical analysis method based on the lattice Boltzmann method (LBM) was developed to aim for better prediction of broadband noise generated from low speed fans. In this study, the validity of the present numerical method for flow analysis in a propeller fan was examined.

In the present numerical method, solid boundaries are treated as immersed boundary using the Interpolated Bounce-Back scheme. The computational grids are generated by the Building-Cube Method (BCM). The grids are refined locally near the solid boundaries based on Cartesian grid. The multi-scale model was introduced into the LBM to allow the calculation with such grids. The present numerical method retains inherent advantages of the LBM such as simple and easy-to-parallelize algorithm.

The flow field of the test propeller fan was simulated by the present numerical method. The number of grid points amounted to about 1.7 billion in total. In the simulation, any subgrid scale models were not introduced explicitly. The LBM results agreed well with the experimental results. In addition, the tip vortex structure calculated by the LBM was consistent with that of detached eddy simulation (DES) which solved the Navier-Stokes equations using a body-fitted grid. The present numerical method was validated to have a capability of successfully simulating the complicated vortical flow field in the propeller fan.

BIBLIOGRAPHY

[1] Marie, S., Ricot, D., Sagut, P. – *Comparison between lattice Boltzmann method and Navier-Stokes high order schemes for computational aeroacoustics*. Journal of Computational Physics, Vol.228, pp.1056-1070, **2009**

[2] Tsutahara, M. – *The finite-difference lattice Boltzmann method and its application in computational aero-acoustics*. Fluid Dynamics Research, Vol.44, No.4, **2012**

[3] V. L. Goff, et al. – *Flow-Induced Noise Predictions of an Automotive Alternator Using a Lattice Boltzmann Method*. Proc. ASME Turbo Expo 2014, GT2014-26386, **2014**

[4] T. Zhu, et al. – *Experimental and Numerical Investigation of Tip Clearance Noise of an Axial Fan Using a Lattice Boltzmann Method*. Proc. the 21th International Congress on Sound and Vibration, **2014**

[5] Guo, Z., Zheng, C., Shi, B. – *Discrete lattice effects on the forcing term in the lattice Boltzmann method*. Physical review E, Vol.65, No.4, **2002**

[6] Filippova, O., Hanel, D. – *Grid refinement for lattice-BGK models*. Journal of Computational Physics, Vol.147, No.1, pp.219-228, **1998**

[7] Bouzidi, M., Firdaouss, M., Lallemand, P. – *Momentum transfer of a Boltzmann-lattice fluid with boundaries*. Physics of Fluids, Vol.13, No.11, pp.3452-3459, **2001**

[8] Gaitonde, D., V., Visbal, M., R. – *Pade-Type higher-order boundary filters for the Navier-Stokes equations*. AIAA-Journal, Vol. 38, No. 11, pp.2103-2112, **2000**

[9] Nakahashi, K. and Kim, L., S. – *Building-cube method for large-scale, high resolution computations*. Proceedings of the 42nd AIAA Aerospace Science Meeting and Exhibit, pp.676-684, **2004**

[10] Kusano, K., Jeong, J., H., Furukawa, M. and Yamada, K. – *Detached eddy simulation of unsteady flow field and prediction of aerodynamic sound in a half-ducted propeller fan*. Proceedings of ASME-JSME-KSME Joint Fluids Engineering Conference 2011, AJK2011-22048, **2011**

[11] Kusano, K., Furukawa, M. and Yamada, K. – *Three-Dimensional Structure of Tip Vortex in a Half-Ducted Propeller Fan.* Transactions of the JSME (in Japanese), Vol. 80, No. 810, **2014**

[12] Sawada, K. – *A Convenient Visualization Method for Identifying Vortex Centers*. Transactions of the Japan society for Aeronautical and Space Sciences, Vol. 38, No. 120, pp. 102-116, **1995**